ACS OMEGA

http://pubs.acs.org/journal/acsodf

Article

Ultrasonication-Assisted Preparation of a Mn-Based Blast Furnace Slag Catalyst: Effects on the Low-Temperature Selective Catalytic Reduction Denitration Process

Zhang Lei,* Kuang Wei, Jia Yang, Lei Zhang, Xi Lu, and Bai Fang

Cite This: *ACS Omega* 2021, 6, 23059−23066

Read Online

ACCESS | Metrics & More | Article Recommendations

ABSTRACT: Reducing costs and improving performance have always been hotspots in the field of catalyst research. In order to control the NO_x in the low-temperature flue gas of nonpower industries, this paper studies the denitration performance of the ultrasonication-assisted preparation of Mn-based blast furnace slag selective catalytic reduction (SCR) low-temperature denitration catalysts. The catalyst was characterized by FT-IR, XRD, and SEM. The study found that ultrasound assistance can make the active components on the catalyst surface more uniformly dispersed and improve the catalytic activity of the catalyst. Under conditions of 80 W ultrasonic power and 20 min ultrasonic time, the denitration performance of the Mn-based blast furnace slag catalyst is optimal, and the NO removal rate is 2.5 times that of the unsonicated catalyst. This work clarified the mechanism of the effect of ultrasonic assistance on the Mn-based blast furnace slag catalyst and at the same time realized the utilization of solid waste resources and air pollution control.

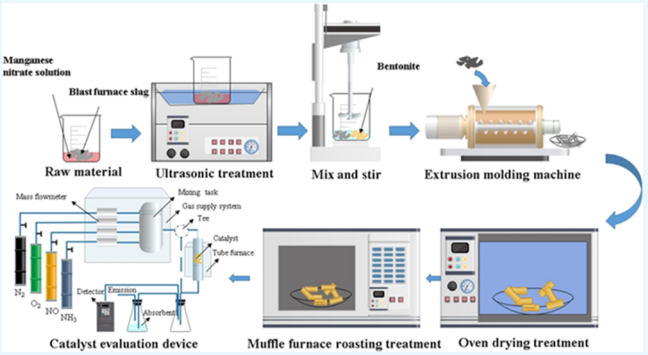

1. INTRODUCTION

Nitrogen oxide (NO_x) is one of the major atmospheric pollutants, which can cause $PM_{2.5}$ and ozone pollution.[1−3] It will lead to a series of environmental problems such as haze, acid rain, photochemical smog, ozone layer destruction, and ozone exceeding the standard, which is harmful to human life and health.[4−7] There are two main sources of NO_x, which are produced in nature and produced by human activities. Most of the NO_x are mainly produced by human activities, including stationary source (coal) combustion[8,9] and mobile source (motor vehicle) combustion.[10] In recent years, due to the popularization of high-efficiency three-way catalysts and denitration devices in coal-fired power plants, NO_x has been controlled to a certain extent.[11] However, in industries such as steel, coking, cement, glass, and ceramics,[12−16] NO_x pollution is still serious.

NO_x control technology includes denitration before combustion, denitration during combustion (low excess air, segmented combustion, flue gas recirculation, and low NO_x combustion) and denitration after combustion (selective noncatalytic reaction, nonselective catalytic reaction, electric beam radiation, selective catalytic reaction, and absorption method).[17−22] The first two technologies have not been used in the actual production process due to their high cost or poor NO_x reduction effect. At present, the postcombustion denitration technology is recognized as the more mature and most promising denitration technology, and the most widely used is the vanadium−titanium-type catalyst selective catalytic reduction (SCR) denitration technology.[23,24] However, it has some disadvantages, such as a narrow active temperature window (280−450 °C), high catalyst toxicity, and deposition of ammonium nitrate.[25,26] Therefore, it is of great significance to develop catalysts with low-temperature activity, weak catalyst toxicity, and high catalytic efficiency.

Mn-based catalysts have redox properties due to the wide valence state distribution of active components and the mutual conversion of manganese between different valence states, which enable NH_3 to selectively reduce NO and promote the SCR reaction.[27,28] Therefore, it has received extensive attention from domestic and foreign scholars.[29−32] Studies have found that Mn-based catalysts have higher low-temperature SCR activity, and the denitration effect can be improved by doping with other transition metals.[33−35] Li found that the supported Mn_2O_3 SCR catalyst can achieve a higher nitrogen oxide removal rate at low temperatures (150−300 °C).[36] Liu

Received: April 18, 2021
Accepted: August 9, 2021
Published: August 31, 2021

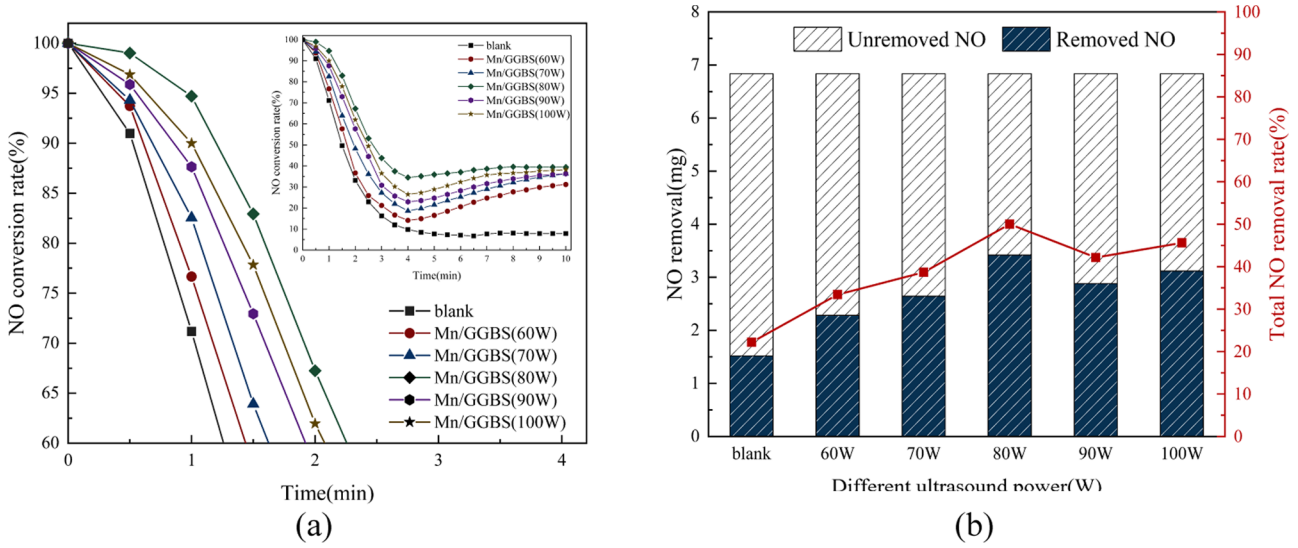

Figure 1. Effect of ultrasonic power on denitration performance of GGBS catalysts. (a) Relationship between NO conversion rate and time. (b) NO removal rate.

studied the selective reduction of NO in flue gas at low temperature and found that manganese in the supported transition-metal oxides has the best denitration effect.[37] The denitration mechanism of the Mn-based SCR denitration catalyst is as follows: NH_3 is first adsorbed by the B acid center Mn−OH, which nears Mn^{4+}═O to form NH^{4+}; NH^{4+} is then attacked by the gas-phase NO to form N_2, H_2O, and Mn^{3+}−OH. Finally, Mn^{3+}−OH was oxidized by O_2 to regenerate Mn^{4+}.[38]

Blast furnace slag is produced by melting and quenching of iron ore and contains CaO, MgO, Al_2O_3, SiO_2, and other substances. With the development of the steel industry, the output of blast furnace slag continues to increase. As a kind of solid waste, blast furnace slag will cause environmental pollution and waste of resources if it is not handled properly. Currently, blast furnace slag is used in the field of construction materials, such as cement, concrete, and roadbed materials.[39] The oxides CaO, MgO, SiO_2, Al_2O_3, Fe_2O_3, and so forth in the blast furnace slag account for more than 80%, so the blast furnace slag is also used in the preparation of photocatalysts, adsorbents, curing materials, and other environmental fields.[40,41]

The active components dispersed on the surface of the carrier can optimize the performance of the catalyst, and ultrasonic treatment can achieve this goal. Ultrasound is a short wave with high energy due to vibration. Ultrasonic waves propagate as longitudinal waves in the medium, so some physical and chemical effects will occur during the propagation process.[42] It mainly includes mechanical effects, acoustic accepted effects, and chemical thermal effects.[43−47]

Blast furnace slag has been widely studied in the field of photocatalysts but less research in the field of denitration. At present, the research on ultrasonication-assisted enhancement of the denitration mechanism of blast furnace slag catalysts has not been reported yet. In this paper, low-cost solid waste ground granulated blast-furnace slag (GGBS) is used as the raw material, and manganese-based SCR denitration catalyst is prepared by ultrasound. For simulating low-temperature SCR process conditions, the effect of ultrasound assistance on the denitration performance of a manganese-based SCR denitration catalyst was investigated. By simulating the low-temperature SCR process conditions, the denitration performance of the GGBS catalyst prepared by ultrasound was evaluated to clarify that it is feasible to improve the denitration performance of the GGBS catalyst with the aid of ultrasound. This work can not only increase the utilization value of blast furnace slag but also improve the catalytic efficiency of the catalyst while realizing the utilization of solid waste resources and air pollution control.

2. RESULTS AND DISCUSSION

2.1. Impact of Denitration Performance. *2.1.1. Effect of Different Ultrasonic Powers on Denitration Performance of GGBS.* The GGBS modified with different ultrasonic powers assisted by manganese nitrate was marked as Mn/GGBS (60 W), Mn/GGBS (70 W), Mn/GGBS (80 W), Mn/GGBS (90 W), and Mn/GGBS (100 W). The prepared catalyst was placed in a denitration experimental device to test the denitration performance, and the result is shown in Figure 1.

It can be seen from Figure 1a that within a certain range, the denitration rate of the catalyst increases with the increase of the ultrasonic power, and the effect is best when the power is 80 W. The reason is that when the ultrasonic power is small, the cavitation effect of ultrasound is small. The mechanical collision force between manganese nitrate and slag is not enough and the reaction is not sufficient, so the active components are not uniformly loaded on the GGBS. However, when the ultrasonic power is too large, the combination of active components and GGBS is inhibited, and its denitration performance will be reduced. The reason is that the microbubbles in the manganese nitrate solution exceed the critical pressure after the tensile stress expands to the outside and the part where the bubble cavity is formed collapses to produce new microbubbles, which affects the denitration performance of the blast furnace slag. It can be seen in Figure 1b that when the power is 80 W, the total NO removal rate has reached 50.03%.

2.1.2. Influence of Different Ultrasonic Times on Denitration Performance of GGBS. Based on the preferred ultrasonic power of 80 W, GGBS catalysts with different ultrasonic times (5, 10, 15, 20, and 25 min) were prepared. The GGBS modified by different ultrasonic times is recorded

https://doi.org/10.1021/acsomega.1c02066
ACS Omega 2021, 6, 23059−23066

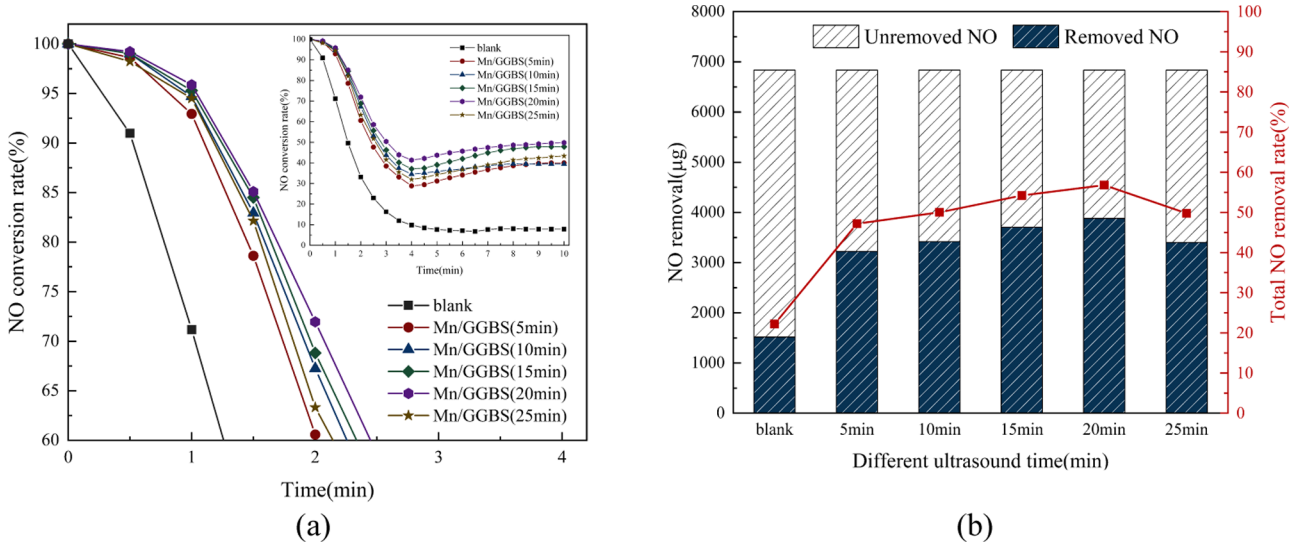

Figure 2. Effect of ultrasonic time on denitration performance of GGBS catalysts. (a) Relationship between the NO conversion rate and time. (b) NO removal rate.

as Mn/GGBS (5 min), Mn/GGBS (10 min), Mn/GGBS (15 min), Mn/GGBS (20 min), and Mn/GGBS (25 min). The superprepared catalyst was placed in the denitration experimental device to test the denitration performance, and the results are shown in Figure 2.

It can be seen in Figure 2a that within a certain range, the denitration rate of the catalyst increases with the increase of the ultrasonic time. When the ultrasonic time is 20 min, the denitration rate reaches the maximum. The reason is that when the ultrasound time is short, the cavitation effect and degree of ultrasound are insufficient, and the active components do not fully make contact with the GGBS. However, when the ultrasound time is too long, the generated microbubbles will expand to the outside, which will reduce the specific surface area of the catalyst, thereby reducing the catalytic activity. It can be seen from Figure 2b that when the time is 20 min, the cumulative denitration amount is the largest, and the total NO removal rate is 56.81%.

2.2. Microstructure Characterization. *2.2.1. Specific Surface Area and Pore Structure Analysis.* The catalyst prepared under the optimum ultrasound conditions is recorded as Mn/GGBS (U) (fresh), and the conventional mixed catalyst is recorded as Mn/GGBS (fresh), and the sample is rejected by Mn/GGBS (U) (inactivated). Table 1 is GGBS and prepared

Table 1. BET and Pore Size in Different Catalysts

catalyst	pore size (nm)	pore volume ($cm^3 \cdot g^{-1}$)	A_{BET} ($m^2 \cdot g^{-1}$)
GGBS	4.259	0.007	2
Mn/GGBS (U) (fresh)	4.132	0.051	21
Mn/GGBS (fresh)	3.752	0.039	15
Mn/GGBS (U) (inactivated)	3.914	0.043	16

catalyst Mn/GGBS (U) (fresh), Mn/GGBS (fresh), Mn/GGBS (inactivated) average aperture, pore volume, and specific surface area. It is known that the aperture of the ultrasonic prepared catalyst is smaller than the catalyst prepared by the raw material GGBS and conventional methods. This is due to the cavitation of ultrasonic waves causing extrusion and expansion in the blast furnace slag powder and solution. This will cause the droplets immersed in the slag to form tiny bubble cavities inside the slag. The physical and chemical properties of the cavitation can improve their aperture distribution, so the ultrasound can improve the specific surface area and aperture volume of the catalyst to a certain extent. After the catalyst is denitrified, the pore structure and the specific surface area are reduced due to ammonium nitrate or sulfate, blocking pores on the surface of the catalyst.

Figure 3 is a N_2 adsorption−desorption and aperture distribution curve of GGBS and Mn/GGBS (U) (fresh). The

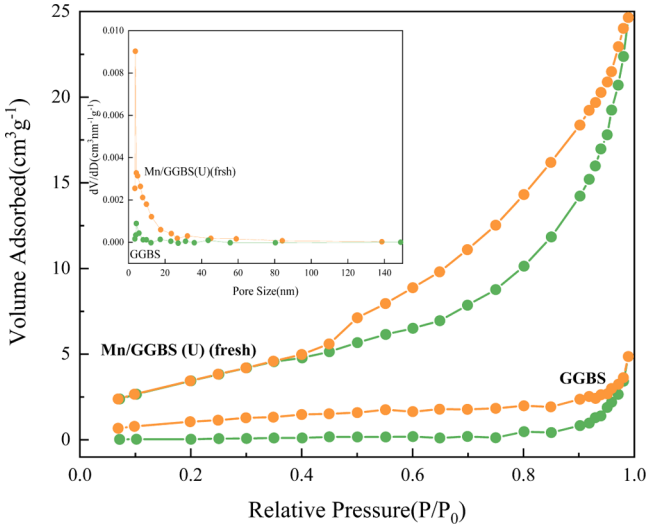

Figure 3. N_2 adsorption and desorption of GGBS and GGBs (U) (fresh) catalysts.

overall adsorption−desorption curves of GGBS and Mn/GGBS (U) (fresh) are of type IV isotherms, and the hysteresis loop is of type H3. Due to the strong interaction of the adsorbate on the surface, the adsorption capacity rises rapidly at a lower relative pressure, and the curve is convex. The latter section of the curve will bulge again, and the middle section may have an adsorption hysteresis loop. Porous adsorbents

https://doi.org/10.1021/acsomega.1c02066
ACS Omega 2021, 6, 23059−23066

show capillary agglomeration, and the curve rises faster due to the occurrence of capillary agglomeration. H3 hysteresis loops are commonly found in aggregates of layered structures and mesoporous materials that produce slits. The adsorption branch is similar to the type II adsorption isotherm, and the lower limit of the desorption branch is usually located at the P/P_0 pressure point caused by cavitation. This type of hysteresis ring is a typical feature of nonrigid aggregates of flake particles, which are slit holes formed by the accumulation of flake particles. GGBS and Mn/GGBS (U) (fresh) did not show adsorption saturation in the higher relative pressure region. Ultrasonic cavitation increases the specific surface area of the catalyst.

2.2.2. FT-IR Analysis. The infrared spectra before and after denitration are shown in Figure 4. At 3800−3500 cm^{-1} is the

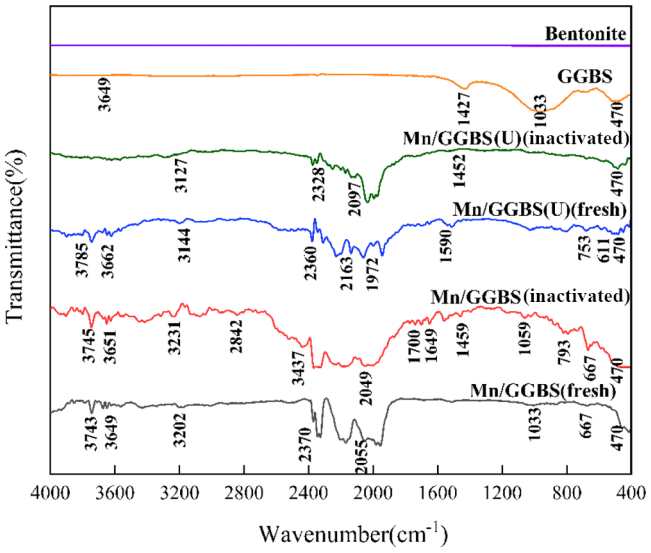

Figure 4. Infrared spectrum of the GGBS catalyst and raw materials.

stretching vibration peak of −OH in the slag hydration product $Ca(OH)_2$. There are multiple single and double peaks in the range of 3300−2000 cm^{-1}, and the HCO_3− absorption peak is in this range. The interval between 1900−1700 cm^{-1} is the position of the absorption peak of $H_2PO_4^-$. 1700−1600 cm^{-1} is the flexural vibration peak position of −OH containing water. 1530−1320 cm^{-1} is the O−C−O stretching vibration peak in CO_3^{2-}, after denitration, CO_3^{2-} is located at 1459 cm^{-1}. Near 1059 cm^{-1} is the peak generated by the stretching vibration of Si−O. The peak of the silicon-containing group is before 900 cm^{-1}, and the absorption peak of bending vibration of Si−O−Si is between 600−400 cm^{-1}. Compared with the catalyst prepared by the conventional mixing method, the catalyst prepared with the aid of ultrasound has reduced peaks in the characteristic region. The reason is that the absorption peak of HCO_3^- in the range of 3300−2000 cm^{-1} reacts with the stretching vibration peak of −OH in the range of 3800−3500 cm^{-1}, and the absorption peak less than 900 cm^{-1} has a small deviation. The peaks of the catalyst prepared by the ultrasonic method after denitration are significantly reduced. This indicates that the functional groups of the catalyst prepared by the ultrasonic method participate in the reaction and are consumed.

2.2.3. XRD Analysis. The Mn-based GGBS prepared by the ultrasonication-assisted method is recorded as Mn/GGBS (U) catalyst, and the XRD patterns of samples Mn/GGBS (U) (fresh) and Mn/GGBS (U) (inactivated) before and after denitration are drawn, as shown in Figure 5.

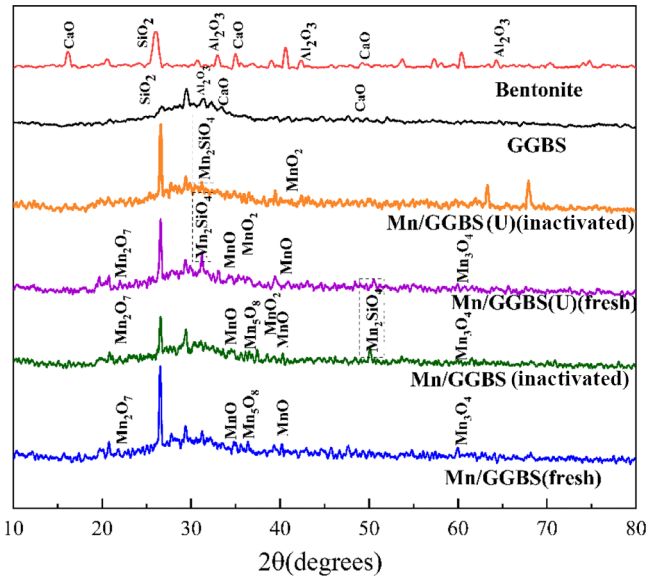

Figure 5. XRD patterns of GGBS catalyst and raw materials.

It can be seen from the figure that the main components of GGBS and bentonite are CaO, Al_2O_3, and SiO_2.The Mn/GGBS (fresh) sample contains abundant manganese oxide crystal structures, including MnO, Mn_3O_4, Mn_2O_7, Mn_5O_8, MnO_2, and Mn_2O_3, have no obvious diffraction peaks. It shows that MnO_2 and Mn_2O_3 are uniformly or amorphously distributed on the surface of the catalyst. After the denitration of the catalyst Mn/GGBS (inactivated), the diffraction peaks everywhere are weakened to varying degrees, and only 37.263° is the diffraction peak of the newly formed MnO_2 (PDF#89-5171). In addition, the GGBS catalyst formed a silicate crystal structure (50.285°) after the denitration reaction. Due to the occurrence of side reactions, the denitration reaction will be affected.

The number of Mn/GGBS(U) (fresh) crystal structures of the catalyst after ultrasonic treatment is reduced, and the corresponding characteristic peak of manganese oxide is relatively weakened. This indicates that manganese is more uniformly dispersed on the surface of the catalyst after ultrasonic treatment. The catalyst after ultrasonic treatment still has no obvious diffraction peak of Mn_2O_3. This shows that Mn_2O_3 does not form a crystal structure; it is amorphous or uniformly dispersed on the surface of the catalyst. Due to the cavitation effect of ultrasound and active $[SiO_4]^{4-}$, the catalyst prepared by the ultrasound-assisted method showed a characteristic peak of Mn_2SiO_4 at 31.174°. 35.236 and 40.912° have weak characteristic peaks of MnO (PDF#75-0257), 37.627° is the characteristic peak of MnO_2 (PDF#72-1982). After denitration, the characteristic peak of manganese oxide is significantly weakened, and the characteristic peak of Mn_2SiO_4 at 31.174° is also weakened. 42.401° is the weak characteristic peak of MnO_2 (PDF#30-0820). The obvious characteristic peaks appearing between 60 and 70° may be formed by complex reactions with other components in the slag.

https://doi.org/10.1021/acsomega.1c02066
ACS Omega 2021, 6, 23059−23066

2.2.4. SEM Analysis. The scanning electron micrographs of the manganese-based GGBS catalyst without ultrasonic treatment (a), the manganese-based GGBS catalyst Mn/GGBS (U) after ultrasonic treatment (b), and GGBS (c) are shown in Figure 6. GGBS varies in size, presents irregular lumps, has a smooth surface, and contains many fine particles. The prepared manganese-based GGBS catalyst does not have distinct edges and small particles in the form of crumbs and appears lamellar at high magnification. After loading manganese salt, the large particles appear to be delaminated. This can effectively increase the specific surface area of the catalyst and improve the catalytic performance. The surface of the ultrasonically treated catalyst particles is relatively smooth, and there is no obvious boundary between the particles. This is because the mechanical action of ultrasound has excellent mass transfer ability at the solid−liquid interface, which promotes the uniform dispersion of manganese nitrate in the GGBS. In addition, the vibration and propagation of ultrasound in the medium will produce a certain amount of friction, which will smoothen the GGBS particles due to friction.

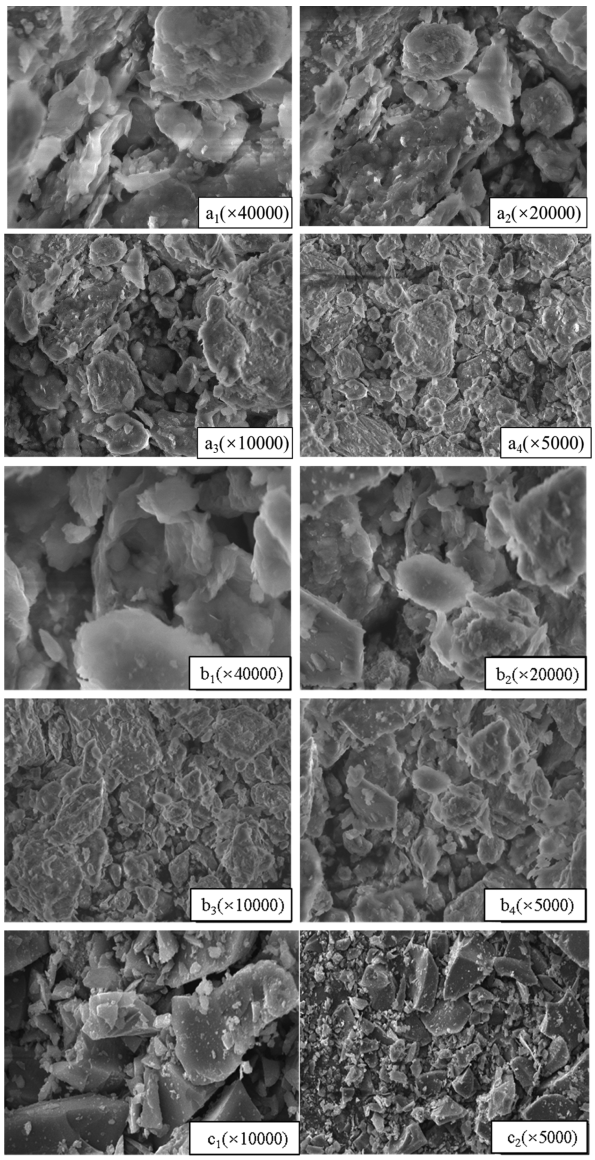

Figure 6. SEM micrographs of different materials. (a) Unsonicated GGBS catalyst. (b) Ultrasound-treated GGBS catalyst. (c) GGBS.

3. CONCLUSIONS

In this paper, GGBS is used as a raw material, and ultrasound-assisted preparation of a manganese-based SCR denitration catalyst is described. By simulating low-temperature SCR process conditions, the effect of ultrasonic assistance on the denitration performance of the manganese-based SCR denitration catalyst was explored. The result shows that the beneficial effects that can be obtained by using ultrasonic treatment in catalyst synthesis. Under the conditions of ultrasonic power of 80 W and ultrasonic time of 20 min, the denitration performance of the Mn-based GGBS catalyst is optimal, and the total NO removal rate has reached 56.81%, and the denitration rate is 2.5 times that of the untreated blast furnace. Through N_2 adsorption−desorption, FT-IR, XRD, and SEM analyses, it is found that ultrasonic treatment can make the surface of the catalyst particles smoother, the distribution of active components is more uniform, and it is easier to participate in the catalytic reaction.

4. EXPERIMENTAL SECTION

4.1. Preparation of the GGBS Catalyst. The GGBS used in the experiment is granulated blast furnace slag powder after vertical milling, produced in a steel plant in Hanzhong, Shaanxi, China. The main chemical components of GGBS are CaO, SiO_2, Al_2O_3, and MgO, and the corresponding percentages are 41.46, 30.19, 13.34, and 7.68%, respectively.[48] The main mineral component of bentonite is montmorillonite, which is produced by Tianyuan Non-Metallic Products Co., Ltd. Manganese nitrate is produced from Tianjin Dengfeng Chemical Reagent Factory. The preparation process of the denitration catalyst by the traditional mixing method was as follows: dissolve manganese nitrate in water according to a 5% load and add GGBS and bentonite (the quality of bentonite is one-fourth of the blast furnace slag powder), and mix the materials thoroughly with a mixer for 30 min. Then, put it into the catalyst molding machine for extrusion molding. The formed catalyst was dried in an oven at 100 °C for 1 h, cut into small columns of about 0.5 cm, and then transferred to a muffle furnace at 400 °C for 2 h. The preparation of the denitration catalyst by ultrasonication-assisted method was as follows: dissolve manganese nitrate in water according to a 5% load, add GGBS, and then place it in an ultrasonic device to adjust the ultrasonic power (60, 70, 80, 90, and 100 W) and ultrasonic time (5, 10, 15, 20, and 25 min). Dry the modified GGBS, add bentonite (the quality of bentonite is a quarter of the GGBS powder) and water, and mix and stir for 30 min. The material is extruded, dried, and roasted to make a denitration catalyst. The muffle furnace is produced by Luoyang Bright Test Electric Furnace Co., Ltd., and the model is BLMT-1400. The ultrasonic instrument is produced by Kunshan Ultrasonic Instrument Co., Ltd., and the model is KQ-500DE.

4.2. Catalyst Evaluation. Test the catalyst activity by simulating the industrial denitration environment. Simulated gas was introduced to observe the changes of its NO data. Set the denitration temperature to 150 °C. Turn on the gas supply system, set O_2 to 6% (60 mL/min), NH_3 to 510 ppm (15 mL/min), NO to 510 ppm (15 mL/min), and remaining filling gas N_2 to 910 mL/min. Insert the Testo (flue gas analyzer) probe

https://doi.org/10.1021/acsomega.1c02066
ACS Omega 2021, 6, 23059−23066

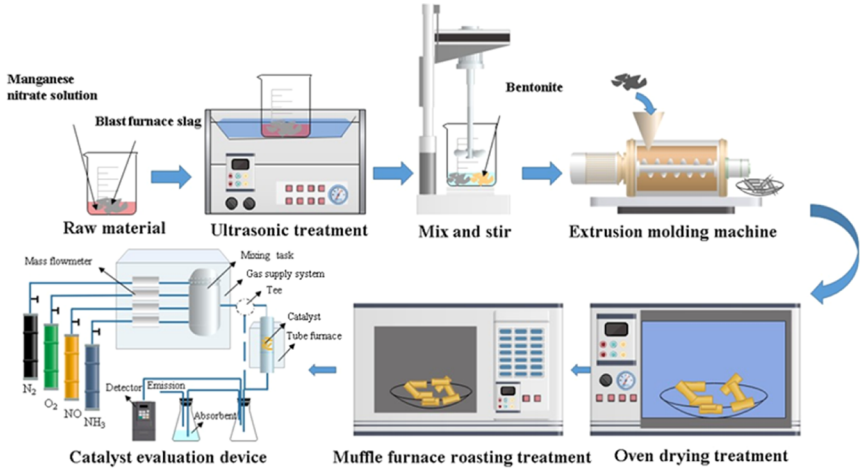

Figure 7. Catalyst preparation method and evaluation.

in the side channel, and put 30 g of the catalyst into the denitration experimental device. After the system is stable, open the tee at the front end of the denitration experimental device to allow the simulated gas to enter the main gas path and the denitration experimental device from the bypass, and then, detect the NO concentration at the outlet. The catalyst was analyzed by N_2 adsorption−desorption, FT-IR, XRD, and SEM. The JW-BK122W high-precision specific surface area and pore analyzer of Beijing Jingwei Gaobo Science and Technology Co., Ltd. was used to analyze the specific surface area and pore structure of the sample. The adsorption conditions are nitrogen adsorption at 77 K, and the relative pressure P/P_0 ranges from 0.005 to 0.99 and 0.00001 to 0.99. The FT-IR spectrometer was produced by Bruker, and the model was VERTEX 70. The X-ray diffraction analyzer used is produced by Beijing Puxi General Instrument Co., Ltd., and the model is XD2/3. Operating conditions: start angle is 3°; end angle is 90°; step width is 0.02; the wavelength is 1.788972, Fe target, working voltage is 36 kV, current is 20 mA. The scanning electron microscope used was produced by JEOL Co., Ltd., and the model was JSM6460LV. The preparation method and evaluation of the catalyst are shown in Figure 7.

AUTHOR INFORMATION

Corresponding Author

Zhang Lei − *School of Geology and Environment, Xi'an University of Science and Technology, Xi'an 710054, China; Key Laboratory of Coal Resources Exploration and Comprehensive Utilization, Ministry of Natural Resources, Xi'an 710021, China;* orcid.org/0000-0001-7145-5588; Phone: +8618502993567; Email: 136750178@qq.com

Authors

Kuang Wei − *School of Geology and Environment, Xi'an University of Science and Technology, Xi'an 710054, China*

Jia Yang − *School of Water Resources and Hydroelectric Engineering, Xi'an University of Technology, Xi'an 710048, China*

Lei Zhang − *China National Heavy Machinery Research Institute Co, Lto, Xi'an 710032, China*

Xi Lu − *School of Geology and Environment, Xi'an University of Science and Technology, Xi'an 710054, China*

Bai Fang − *CAS Key Laboratory of Green Process and Engineering, Institute of Process Engineering, Chinese Academy of Sciences, Beijing 100190, China*

Complete contact information is available at: https://pubs.acs.org/10.1021/acsomega.1c02066

Author Contributions

Conceptualization, Z. L. and L. Z.; methodology, K. W.; software, J. Y. and X. L.; validation; investigation, J. Y.; data curation, J. Y.; writing-original draft preparation, K. W.; writing-review and editing, K. W.; article language check edit, B. F..

Notes

The authors declare no competing financial interest.
Declarations of interest: None.

ACKNOWLEDGMENTS

This research was funded by the Key Research and Development Program of Shaanxi (2019ZDLSF05-05-01), Natural Science Basic Research Program of Shaanxi (2019JL-01), Xi'an Science and Technology Plan project (2019217714GXRC013CG014-GXYD13.4), Open Fund of Shaanxi Key Laboratory of Geological Support for Coal Green Exploitation (DZBZ2020-03), Xi'an University of Science and Technology, and State Key Laboratory of Coal Resources in Western China (SKLCRKF20-15).

REFERENCES

(1) Park, S.; Choe, W.; Jo, C. Interplay among ozone and nitrogen oxides in air plasmas: Rapid change in plasma chemistry. *Chem. Eng. J.* **2018**, *352*, 1014−1021.

(2) Ren, Z.; Zhang, H.; Wang, G.; Pan, Y.; Yu, Z.; Long, H. Effect of Calcination Temperature on the Activation Performance and Reaction Mechanism of Ce-Mn-Ru/TiO_2 Catalysts for Selective Catalytic Reduction of NO with NH_3. *ACS Omega* **2020**, *5*, 33357−33371.

(3) Yang, X.; Wang, X.; Qiao, X.; Jin, Y.; Fan, B. Effect of Hydrothermal Aging Treatment on Decomposition of NO by Cu-ZSM-5 and Modified Mechanism of Doping Ce against This Influence. *Materials* **2020**, *13*, 888.

(4) Mason, M. M.; Lee, Z. R.; Vasiliu, M.; Wachs, I. E.; Dixon, D. A. Initial Steps in the Selective Catalytic Reduction of NO with NH_3 by TiO_2-Supported Vanadium Oxides. *ACS Catal.* **2020**, *10*, 13918−13931.

(5) Wang, H.; Zhang, L.; Tian, Y.; Jia, Y.; Bo, G.; Luo, L.; Liu, L.; Shi, G.; Li, F. Performance of nitrobenzene and its intermediate aniline removal by constructed wetlands coupled with the micro-electric field. *Chemosphere* **2021**, *264*, 128456.
(6) Lei, Z.; Yang, J.; Hao, S.; Xin, W.; Min, L.; Yusu, W.; Dan, X. Application of Surfactant-modified Cordierite-based Catalysts in Denitration Process. *Fuel* **2020**, *268*, 117242.
(7) Wang, H.; Wang, J.; Bo, G.; Wu, S.; Luo, L. Degradation of pollutants in polluted river water using Ti/IrO_2-Ta_2O_5 coating electrode and evaluation of electrode characteristics. *J. Clean. Prod.* **2020**, *273*, 123091.
(8) Zhao, H.; Li, Y.; Song, Q.; Liu, S.; Ma, L.; Shu, X. Catalytic reforming of volatiles from co-pyrolysis of lignite blended with corn straw over three iron ores: Effect of iron ore types on the product distribution, carbon-deposited iron ore reactivity and its mechanism. *Fuel* **2021**, *286*, 119398.
(9) Zhao, H.; Song, Q.; Liu, S.; Li, Y.; Wang, X.; Shu, X. Study on catalytic co-pyrolysis of physical mixture/staged pyrolysis characteristics of lignite and straw over an catalytic beds of char and its mechanism. *Energy Convers. Manag.* **2018**, *161*, 13−26.
(10) Xu, C.; Hong, J.; Ren, Y.; Wang, Q.; Yuan, X. Approaches for controlling air pollutants and their environmental impacts generated from coal-based electricity generation in China. *Environ. Sci. Pollut. Res.* **2015**, *22*, 12384−12395.
(11) Chen, Y.; Deng, J.; Fan, J.; Jiao, Y.; Wang, J.; Chen, Y. Key role of NO + C_3H_8 reaction for the elimination of NO in automobile exhaust by three-way catalyst. *Environ. Sci. Pollut. Res.* **2019**, *26*, 26071−26081.
(12) Lei, Z.; Hao, S.; Yang, J.; Lei, Z.; Dan, X. Study on Solid Waste Pyrolysis Coke Catalyst for Catalytic Cracking of Coal Tar. *Int. J. Hydrogen Energy* **2020**, *45*, 19280−19290.
(13) Li, Y.-h.; Chang, F.-m.; Huang, B.; Song, Y.-p.; Zhao, H.-y.; Wang, K.-j. Activated carbon preparation from pyrolysis char of sewage sludge and its adsorption performance for organic compounds in sewage. *Fuel* **2020**, *266*, 117063.
(14) Song, Q.; Zhao, H.; Jia, J.; Yang, L.; Lv, W.; Bao, J.; Shu, X.; Gu, Q.; Zhang, P. Pyrolysis of municipal solid waste with iron-based additives: A study on the kinetic, product distribution and catalytic mechanisms. *J. Clean. Prod.* **2020**, *258*, 120682.
(15) Song, Q.; Zhao, H.; Chang, S.; Yang, L.; Zou, F.; Shu, X.; Zhang, P. Study on the catalytic pyrolysis of coal volatiles over hematite for the production of light tar. *J. Anal. Appl. Pyrol.* **2020**, *151*, 104927.
(16) Song, Q.; Zhao, H.; Jia, J.; Yang, L.; Lv, W.; Gu, Q.; Shu, X. Effects of demineralization on the surface morphology, microcrystalline and thermal transformation characteristics of coal. *J. Anal. Appl. Pyrol.* **2020**, *145*, 104716.
(17) Wang, H.; Quan, B.; Bo, G.; Zhang, Y.; Liu, L.; Zhang, J.; Zhang, X.; Zhang, C. Advanced oxidation treatment of dissolved organic matter from wastewater treatment plant secondary effluent using scattering electrical reactor. *J. Clean. Prod.* **2020**, *267*, 122258.
(18) Mundhwa, M.; Thurgood, C. P. Numerical study of methane steam reforming and methane combustion over the segmented and continuously coated layers of catalysts in a plate reactor. *Fuel Process. Technol.* **2017**, *158*, 57−72.
(19) Zhang, L.; Jia, Y.; Shu, H.; Zhang, L.; Lu, X.; Bai, F.; Zhao, Q. Y.; Tian, D. The effect of basicity of modified ground granulated blast furnace slag on its denitration performance. *J. Clean. Prod.* **2021**, *305*, 126800.
(20) Zhang, Y.; Krasheninnikov, S. I. Electron dynamics in the laser and quasi-static electric and magnetic fields. *Phys. Lett. A* **2018**, *382*, 1801−1806.
(21) Zhang, J.; Sun, G.; Liu, J.; Evrendilek, F.; Buyukada, M. Co-combustion of textile dyeing sludge with cattle manure: Assessment of thermal behavior, gaseous products, and ash Characteristics. *J. Clean. Prod.* **2020**, *253*, 119950.
(22) Chen, J.; Zhang, J.; Liu, J.; He, Y.; Evrendilek, F.; Buyukada, M.; Xie, W.; Sun, S. Co-pyrolytic mechanisms, kinetics, emissions and products of biomass and sewage sludge in N_2, CO_2 and mixed atmospheres. *Chem. Eng. J.* **2020**, *397*, 125372.
(23) Lei, Z.; Lingbo, Q.; Hao, S.; Yang, J.; Lei, Z.; Chao, Y.; Fang, B.; Zhiyu, S. Formation of fly ash catalyst and selection of matrix binder and its application in denitration. *ACS Omega* **2020**, *5*, 31567−31574.
(24) Lei, Z.; Hao, S.; Yang, J.; Zhang, L.; Fang, B.; Wei, K.; Lingbo, Q.; Jin, S.; Wei, C. Study on denitration and sulfur removal performance of Mn−Ce supported fly ash catalyst. *Chemosphere* **2021**, *270*, 128646.
(25) Wang, J.; Yang, Z.; Wang, H.; Wu, S.; Lu, H.; Wang, X. Decomposition process of cefotaxime sodium from antibiotic wastewater by Up-flow Blanket Filter (UBF) reactor: Reactor performance, sludge characteristics and microbial community structure analysis. *Sci. Total Environ.* **2021**, *758*, 143670.
(26) Wang, H.; Wang, J.; Bo, G.; Wu, S.; Luo, L. Degradation of pollutants in polluted river water using Ti/IrO_2-Ta_2O_5 coating electrode and evaluation of electrode characteristics. *J. Clean. Prod.* **2020**, *273*, 123019.
(27) Gao, C.; Shi, J.-W.; Fan, Z.; Gao, G.; Niu, C. Sulfur and Water Resistance of Mn-Based Catalysts for Low-Temperature Selective Catalytic Reduction of NOx: A Review. *Catalysts* **2018**, *8*, 11.
(28) Nagaiah, T. C.; Tiwari, A.; Kumar, M.; Scieszka, D.; Bandarenka, A. S. In situ Probing of Mn_2O_3 Activation toward Oxygen Electroreduction by the Laser-Induced Current Transient Technique. *ACS Appl. Energy Mater.* **2020**, *3*, 9151−9157.
(29) Li, K.; Chen, J.; Peng, J.; Ruan, R.; Omran, M.; Chen, G. Dielectric properties and thermal behavior of electrolytic manganese anode mud in microwave field. *J. Hazard. Mater.* **2020**, *384*, 121227.
(30) Li, K.; Chen, J.; Peng, J.; Ruan, R.; Srinivasakannan, C.; Chen, G. Pilot-scale study on enhanced carbothermal reduction of low-grade pyrolusite using microwave heating. *Powder Technol.* **2020**, *360*, 846−854.
(31) Li, K.; Jiang, Q.; Chen, G.; Gao, L.; Peng, J.; Chen, Q.; Koppala, S.; Omran, M.; Chen, J. Kinetics characteristics and microwave reduction behavior of walnut shell-pyrolusite blends. *Bioresour. Technol.* **2021**, *319*, 124172.
(32) Li, K.; Chen, J.; Chen, G.; Peng, J.; Ruan, R.; Srinivasakannan, C. Microwave dielectric properties and thermochemical characteristics of the mixtures of walnut shell and manganese ore. *Bioresour. Technol.* **2019**, *286*, 121381.
(33) Qi, Y.; Shan, X.; Wang, M.; Hu, D.; Song, Y.; Ge, P.; Wu, J. Study on Low-Temperature SCR Denitration Mechanisms of Manganese-Based Catalysts with Different Carriers. *Water, Air, Soil Pollut.* **2020**, *231*, 289.
(34) Tang, X.; Wang, C.; Gao, F.; Ma, Y.; Yi, H.; Zhao, S.; Zhou, Y. Effect of hierarchical element doping on the low-temperature activity of manganese-based catalysts for NH_3-SCR. *J. Environ. Chem. Eng.* **2020**, *8*, 104399.
(35) Liu, K.; Yu, Q.; Wang, B.; San, J.; Duan, W.; Qin, Q. Binary copper-manganese based catalysts with urea for low-temperature selective catalytic reduction of NO: Performance, characterization and mechanism. *Appl. Surf. Sci.* **2020**, *508*, 144755.
(36) Li, G.; Wang, B.; Ma, Z.; Wang, H.; Ma, J.; Zhao, C.; Zhou, J.; Lin, D.; He, F.; Han, Z.; Sun, Q.; Wang, Y. Aluminium-induced component engineering of mesoporous composite materials for low-temperature NH_3-SCR. *Chem. Commun.* **2020**, *3*, 66.
(37) Liu, K.; Yu, Q.; Wang, B.; Xie, H.; Duan, W.; Qin, Q. Activated carbon-supported catalyst loading of CH_4N_2O for selective reduction of NO from flue gas at low temperatures. *Int. J. Hydrogen Energy* **2019**, *44*, 13523−13537.
(38) Zhang, L.; Wen, X.; Lei, Z.; Gao, L.; Sha, X.; Ma, Z.; He, H.; Wang, Y.; Jia, Y.; Li, Y. Study on the mechanism of a manganese-based catalyst for catalytic NO_X flue gas denitration. *AIP Adv.* **2018**, *8*, 045004.
(39) Choi, Y. C.; Kim, J.; Choi, S. Mercury intrusion porosimetry characterization of micropore structures of high-strength cement pastes incorporating high volume ground granulated blast-furnace slag. *Constr. Build. Mater.* **2017**, *137*, 96−103.

https://doi.org/10.1021/acsomega.1c02066
ACS Omega 2021, 6, 23059−23066

(40) Meek, A. H.; Beckett, C. T. S.; Elchalakani, M. Alternative stabilised rammed earth materials incorporating recycled waste and industrial by-products: Durability with and without water repellent. *Constr. Build. Mater.* **2020**, *265*, 120629.
(41) Zhang, L.; Jia, Y.; Shu, H.; Zhang, L.; Lu, X.; Bai, F.; Zhao, Q.; Tian, D. The effect of basicity of modified ground granulated blast furnace slag on its denitration performance. *J. Clean. Prod.* **2021**, *305*, 126800.
(42) Patil, V. S.; Gogate, P. R. Ultrasound-assisted improved synthesis of supported V_2O_5 catalyst and subsequent application for the production of n-hexyl acetate. *Chem. Eng. J.* **2016**, *289*, 513−524.
(43) Pi, X.; Sun, F.; Qu, Z.; Gao, J.; Wang, A.; Zhao, G.; Liu, H. Producing elemental sulfur from SO_2 by calcium loaded activated coke: Enhanced activity and selectivity. *Chem. Eng. J.* **2020**, *401*, 126022.
(44) Thari, F. Z.; Tachallait, H.; El Alaoui, N.-E.; Talha, A.; Arshad, S.; Álvarez, E.; Karrouchi, K.; Bougrin, K. Ultrasound-assisted one-pot green synthesis of new N-substituted-5-arylidene-thiazolidine-2,4-dione-isoxazoline derivatives using NaCl/Oxone/Na_3PO_4 in aqueous media. *Ultrason. Sonochem.* **2020**, *68*, 105222.
(45) Sabaghi, M.; Aghajani, Z.; Najafi, G. R. Fabrication of a new heterogeneous tungstate-based on the amino-functionalized metal-organic framework as an efficient catalyst towards sonochemical oxidation of alcohols under green condition. *J. Organomet. Chem.* **2020**, *925*, 121483.
(46) Shi, L.; Zhang, Z.; Wang, R.; Zhou, C.; Sun, C. Study on ultrasound-assisted precipitation for preparing Ni/Al_2O_3 catalyst. *Ultrason. Sonochem.* **2020**, *67*, 105107.
(47) Jeganathan, S.; Kandasamy, K.; Velusamy, S.; Sankaran, P. Comparative studies on ultrasound assisted treatment of tannery effluent using multiple oxy-catalysts using response surface methodology. *Arabian J. Chem.* **2020**, *13*, 7066−7077.
(48) Lu, Z.; Lei, Z.; Hao, S.; Yang, J.; Lei, Z.; Fang, B.; Xiaosheng, C. Study on Denitration Performance of Solid Waste Blast Furnace Slag Catalysts under Different Preparation Processes. *ACS Omega* **2020**, *5*, 32216−32226.

https://doi.org/10.1021/acsomega.1c02066
ACS Omega 2021, 6, 23059−23066